J Solid State Electrochem (2012) 16:1709–1721
DOI 10.1007/s10008-011-1587-1

ORIGINAL PAPER

Natural and synthetic solid polymer hybrid dual network membranes as electrolytes for direct methanol fuel cells

S. Meenakshi · S. D. Bhat · A. K. Sahu · S. Alwin · P. Sridhar · S. Pitchumani

Received: 3 August 2011 / Revised: 26 September 2011 / Accepted: 1 November 2011 / Published online: 17 November 2011

Abstract Hybrid dual-network membranes comprising chitosan (CS)–polyvinyl alcohol (PVA) networks crosslinked with sulfosuccinic acid (SSA) and glutaraldehyde (GA) and modified with stabilized silicotungstic acid (SWA) are reported for their application in direct methanol fuel cells (DMFCs). Physico-chemical properties of these membranes are evaluated using thermo-gravimetric analysis and scanning electron microscopy in conjunction with their mechanical properties. Based on water sorption and proton conductivity measurements for the membranes, the optimum content of 10 wt.% SWA in the membrane is established. The methanol crossover for these membranes are studied by measuring the mass balance of methanol using density meter and are found to be lower compared to Nafion-117 membrane. The membrane–electrode assembly with 10 wt.% stabilized SWA–CS–PVA hybrid membrane with SSA and GA as crosslinking agent delivers a peak power density of 156 mW cm^{-2} at a load current density of 400 mA cm^{-2} and 88 mW cm^{-2} at a load current density of 300 mA cm^{-2}, respectively, in DMFC at 70 °C.

Keywords Hybrid membrane · Silicotungstic acid · Methanol crossover · Direct methanol fuel cell

Introduction

Fuel cell has emerged as a potential energy conversion device that converts chemical energy directly into electricity in comparison to conventional heat engines that produce electricity with reduced efficiency. Proton exchange membrane fuel cells (PEMFCs) have attracted much attention as clean energy sources because of their high power density and efficiency with low emission levels for various applications such as electric vehicles, portable electronics, and residential power generation [1–5]. In view of this, direct methanol fuel cells (DMFCs) have reached a high level of development and are now almost universally referred to as the sixth fuel cell type. In terms of applications, they are set to function as power sources for a range of stationary applications. This position has largely been brought about by the convenience of storage of the liquid fuel. At present, DMFCs employ Nafion, a proton-conducting perfluorosulfonic acid polymer membrane, as electrolyte that also acts as a physical separator to prevent methanol crossover from the anode to the cathode. However, methanol crossover from anode to cathode across the Nafion membrane brings about a mixed potential at the cathode, causing loss of fuel and cell polarization [6–8].

To overcome the abovementioned issues, alternative polymeric membranes have been developed and used as electrolytes to mitigate the methanol crossover for effective DMFC performance. Majority of these membranes are made from solid polymers due to their wide variability of barrier structures and properties [9–11]. In recent years, natural and synthetic polymer composite membranes have made significant impact as polymer electrolytes for DMFCs [12, 13]. Among these, natural polymer chitosan (CS) and synthetic polymer poly (vinyl alcohol) (PVA) have drawn considerable attention in the past decade [14, 15]. CS is the second most abundant natural bio-polymer obtained by alkaline deacetylation of chitin, a major component in the exo-skeleton of crustaceans [16]. Due to its low cost of production, natural abundance, and eco-compatibility, CS is

S. Meenakshi · S. D. Bhat · A. K. Sahu · S. Alwin · P. Sridhar · S. Pitchumani (✉)
CSIR-Central Electrochemical Research Institute—Madras Unit,
CSIR Madras Complex,
Taramani, Chennai 600113, India
e-mail: spmanicecri@gmail.com

a preferred membrane material for ultra-filtration, reverse osmosis, and pervaportion [17–19]. It is also reflected that CS-based natural polymeric composite membranes can help reduce the methanol crossover in DMFCs [20–22]. PVA can also be used as an attractive material for membrane electrolyte in DMFCs owing to its good mechanical and chemical stability [23]. PVA-based blend or composite membranes also offer high electrochemical selectivity in DMFCs [24, 25].

However, CS and PVA suffer from high modulus of elasticity with low strain to break and high crystallinity and hence need to be blended with each other to improve hydrophilicity and mechanical properties [26–29]. CS–PVA blend membranes have been prepared and used for pervaporative dehydration of isopropanol and ethylene glycol [26]. Carboxyethyl CS–PVA nanofibrous membranes have also been used as wound dressing materials for skin regeneration [27]. The effect of chemical crosslinking and formation of single- and dual-network structures in CS–PVA films have also been studied [28]. Wu et al. reported that CS–PVA blend has higher selectivity, mechanical strength, and stability than the pristine PVA membranes [29]. Crosslinking between polymers have to be present to avoid dissolution of hydrophilic polymer chains into aqueous phase. Efficient crosslinking between polymers can be carried out by physical and chemical methods depending on the nature of the polymer [30–32]. The most efficient crosslinking agents for PVA- and CS-based membranes reported in the literature are glutaraldehyde (GA) and sulfosuccinic acid (SSA) [23, 33].

Heteropoly acids (HPAs) are known to be strong Brönsted acids as well as solid electrolytes [34]. For example, certain HPAs, such as phosphomolybdic acid ($H_3PMo_{12}O_{40}$), phosphotungstic acid ($H_3PW_{12}O_{40}$), and silicotungstic acid ($H_4SiW_{12}O_{40}$), possess a unique discrete structure and exhibit high proton mobility [35]. Some reports suggest that incorporation of HPAs into natural polymers, like CS and synthetic polymers like PVA, improves methanol barrier properties [36, 37]. However, high solubility of HPAs in aqueous media and large particle size of the inorganic additives bring about ineffective bridging between the ionic domains, affecting membrane endurance and hence DMFC performance [38, 39]. Hence, stabilized HPAs are prepared by ion-exchanging protons of HPAs with larger cations, such as caesium, followed by their incorporation in polymer matrix to realize effective DMFC performance [40–44].

Our recent findings suggest that PVA-PSSA, modernite (MOR)-incorporated PVA–PSSA with varying degrees of sulfonation, and PVA–SSA–HPA composite membranes exhibit attractive mechanical stability and provide promising DMFC performance [45–47]. It was also found that CS-hydroxyethyl cellulose (HEC), CS-gelatin (GL), and sodium alginate (NaAlg)-PVA blends on modification by incorporating HPAs can be successfully employed as solid polymer electrolyte membranes for DMFCs owing to their low cost and excellent methanol barrier properties in relation to commercially available membranes [40, 48, 49].

However, high degree of swelling and less stability are the limitations of the above membranes. To overcome these issues, the present study is an attempt to fabricate a hybrid dual-network solid polymer electrolyte membrane with interconnected networks of natural polymer CS and a synthetic polymer PVA crosslinked with GA/SSA and incorporated with stabilized silicotungstic acid (SWA) for its application in DMFCs. The solid polymer networks were interconnected through the crosslinked covalent bonds. SWA was stabilized with larger cations using caesium carbonate in the present study.

Experimental

Membrane and electrode materials

CS flakes with M_w of 100,000 (degree of deacetylization> 95%), PVA with M_w of 133,000, SSA, GA solution, SWA (M_w=2878.29 $g\,mol^{-1}$), and caesium carbonate were procured from Aldrich Chemicals. Glacial acetic acid and sulphuric acid were procured from Acros Chemicals. All chemicals were used as received. Toray TGP-H-120 carbon paper was procured from Nikunj Exim Pvt. Ltd., India. Vulcan XC-72R carbon, Pt–Ru (60 wt.% in 1:1 atomic ratio), and Pt/C (40 wt.% Pt on Vulcan XC-72R carbon) were obtained from Alfa Aesar (Johnson Matthey, India) Chemicals. De-ionized (DI) water (conductivity, 18.4 MΩ cm) from the Millipore system was used during the study.

Stabilization of SWA

SWA was stabilized with stoichiometric amounts of caesium carbonate in deionized water similar to the procedure described elsewhere [44]. The transparent, homogenous SWA solution turned cloudy white as it precipitated out on ion exchanging the protons with the larger cations present in the caesium carbonate solution. The resulting mixture was sonicated in an ultrasonic bath for 4 h and allowed to dry in an air oven at 30 °C. SWA thus obtained was heat-treated at 350 °C for 3 h and ground to fine powder. Since SWA is a tribasic acid, attempts were made to control the number of protons substituted by controlling the stoichiometry of the added salt solution, namely, Cs/SWA in 1:0.5 molar ratio, enabling one H^+ ion from SWA to exchange with caesium and to stabilize it in aqueous/acidic medium [47, 50].

Membrane preparation

CS–PVA blend membranes were prepared by varying the composition of CS and PVA and the blend membrane comprising CS–PVA at 75:25 was chosen for further studies based on the water uptake properties of the membrane in agreement with the literature [26]. CS–PVA–Cs–SWA hybrid membranes were prepared by solution casting technique. In brief, 0.75 g of CS was dissolved in 75 ml of 2 wt.% acetic acid with stirring to form a homogeneous viscous solution. A total of 2.5 g of PVA was dissolved in 25 ml of deionized water at 60 °C. PVA and CS are crosslinked with 0.6 ml of SSA and 0.5 ml of GA solution, respectively. Both CS and PVA solutions are mixed together and allowed to stir for 24 h. The required amount of stabilized SWA was ultrasonicated for 2 h and then added to CS–PVA solution to form a hybrid solution. The solutions were cast in a Plexiglass plate and the solvent was evaporated at 30 °C to form a membrane. The membrane was peeled off from the glass plate and washed with deionized water repeatedly to remove the residual impurities and used for further studies. The membrane thickness was measured by thickness dial gauge and was found to be ~170 μm. The addition of stabilized SWA into crosslinked CS–PVA polymer matrix was restricted to 15 wt.% due to the aggregation of SWA particles in the membrane.

Additive stability of SWA and Cs-stabilized SWA in crosslinked CS–PVA membrane

The additive stability in aqueous/acidic media was determined by the procedure reported elsewhere [42]. Hybrid membranes were pre-treated in an oven at 70 °C for 1 h followed by immersing samples of the treated membrane of known weight into hot aqueous H_2SO_4 (1 M/85 °C) for 3 h and subsequently washing with a copious amount of hot DI water (85 °C). The treated membranes were dried in an oven at 70 °C and weighed again, and the difference in weight was taken as the loss of additive.

Sorption measurements

For water sorption measurements, circularly cut (diameter= 2.5 cm) membranes were dipped in de-ionized water for 24 h to attain equilibrium. The samples were surface-dried and their initial mass values were recorded on a single-pan digital microbalance (Sartorius, Germany) within an accuracy of ±0.01 mg. The samples were then dried in a hot-air oven at 70 °C for 24 h and their weights were measured. The % sorption was calculated from Eq. 1 as given below:

$$\%\ \text{Water sorption} = \left(\frac{W_\infty - W_\circ}{W_\circ}\right) \times 100 \tag{1}$$

where W_∞ and W_o are the weights of sorbed and dry membranes, respectively.

Proton conductivity measurements

Proton conductivity measurements were performed on Nafion-117, CS–PVA–SSA–Cs-stabilized SWA and CS–PVA–GA-Cs-stabilized SWA membranes in a two-probe cell by AC impedance technique as described elsewhere [47]. In brief, the conductivity cell comprised two stainless steel electrodes, each of 20 mm in diameter. The membrane sample was sandwiched between the two stainless steel electrodes fixed in a Teflon block and kept in a closed glass container. The ionic conductivity data for the membranes were obtained under fully humidified condition (relative humidity=100%) by keeping de-ionized water at the bottom of the test container and equilibrating around 24 h. Subsequently, conductivity measurements were conducted between 30 °C and 100 °C in a glass container with the provision to heat. The temperature of the conductivity cell was constantly monitored with a thermometer kept inside the container adjacent to the membrane. AC impedance spectra for the membranes were recorded in the frequency range between 1 MHz and 10 Hz with 10 mV amplitude using an Autolab PGSTAT 30. The resistance of the membrane was determined from the high-frequency intercept of the impedance with the real axis. The membrane conductivity was calculated from the membrane resistance, R, from Eq. 2 as given below:

$$\sigma = \frac{l}{RA} \tag{2}$$

where σ is the proton conductivity of the membrane in S cm^{-1}, l is the membrane thickness in cm, and A is the crosssectional area of the membrane samples in cm^2.

Physicochemical characterization

Universal testing machine (Model AGS-J, Shimadzu, China) with an operating head load of 10 kN was used to study the mechanical properties of the membranes. Cross-sectional area for the membranes was obtained from the initial width and thickness of the membrane sample. The test samples were dumbbell-shaped as per ASTM D-882 standards. The sample membrane was then placed in the sample holder and the membrane was stretched at a crosshead speed of 1 mm/min and its tensile strength was estimated from Eq. 3 as given below:

$$\text{Tensile strength (N mm}^{-2}) = \frac{\text{Maximum load}}{\text{Crosssectional area}} \tag{3}$$

Thermo-gravimetric analysis (TGA) for CS–PVA–SSA, CS–PVA–GA, CS–PVA–SSA-Cs-stabilized SWA, and CS–

PVA–GA-Cs-stabilized SWA membranes was conducted using a SDT Q600 V8.2 TGA/DTA Instrument (US) in the temperature range between 0 and 800 °C at a heating rate of 5 °C min^{-1} with nitrogen flushed at 200 ml min^{-1}. Average contact angle and surface wetting energy measurements were conducted on these membranes using a Surface Electro Optics (Model Phoenix-300, Korea) setup by Sessile drop method.

Surface micrographs for crosslinked CS–PVA blend membrane and CS–PVA–Cs-stabilized SWA hybrid membranes were obtained using JEOL JSM 35CF scanning electron microscope (SEM). Gold film of thickness <100 nm was sputtered on the membrane surface using a JEOL Fine Coat Ion Sputter-JFC-1100 unit prior to their examination under SEM.

Methanol permeation studies

Methanol crossover can be measured by measuring the CO_2 concentration in cathode exhaust gases by: (a) mass spectroscopy, (b) gas chromatography, (c) gas analyzer, and (d) CO_2 gas sensor. These measurements do not account for CO_2 permeation across the membrane and hence could be erroneous. The density measurement is free from the abovementioned problem. Determination of methanol crossover using density measurement method has already been reported elsewhere [48].

The permeated methanol from anode to cathode was measured by determining the methanol concentration based on the mass balance between the methanol supplied to the cell, methanol utilized for the electrochemical reaction, and unutilized methanol during the DMFC operation. The approach follows Faraday's law [51], where concentration of methanol varies with the load current density with 1 mol of methanol being equivalent to 96,485 C. Accordingly, the amount of the crossover methanol ($MeOH_{crossover}$) was taken as the difference between the amounts of methanol circulated inside the cell ($MeOH_{cir}$) for the reaction and the methanol consumed during the faradaic reaction to produce electrical energy ($MeOH_{rxn}$).

Aqueous methanol of 2 M was initially supplied to the DMFC and the cell was allowed for equilibration. After attaining steady state, the difference in the amount of methanol supplied to the cell and the methanol collected at the anode outlet for a particular time (t) was measured under open-circuit voltage (OCV) condition at 70 °C. The densities of methanol collected from the inlet and outlet of the cell anode were measured using a density meter (Mettler Toledo DE51) with 20 ml of the collected methanol sample. Subsequent to each measurement, the density meter was rinsed with water and isopropanol followed by aqueous methanol solution. The molarity of the methanol was calculated from the measured density values using Eq. 4 [52].

$$\text{Molarity} = 10 \times \text{wt.\% of methanol}\left(\frac{\rho}{M}\right) \tag{4}$$

In Eq. 4, ρ is the density of methanol (g cm^{-3}) and M is the molecular weight of methanol (g mol^{-1}).

Concentration (C_1) and volume (V_1) of the inlet methanol and the methanol concentration (C_2) and volume (V_2) of the outlet methanol were measured separately after the cell operation was stopped. It is noteworthy that, under OCV condition, methanol supplied at the inlet ($MeOH_{in}$) was equal to the sum of the methanol collected at the outlet ($MeOH_{out}$) and the methanol crossed over ($MeOH_{crossover}$) from the anode to the cathode side of the cell. Accordingly:

$$MeOH_{crossover} = MeOH_{in} - MeOH_{out} \tag{5}$$

At a particular current density (I), methanol consumed during the electrochemical oxidation reaction over time (t) was calculated to be 4.19×10^{-3} ml A^{-1} min^{-1} from Eq. 6.

$$MeOH_{rxn} = I \times 4.19 \times 10^{-3} \times t \tag{6}$$

In Eq. 6, I is in A and t is in min. Crossover methanol was calculated using Eqs. 5 and 6. Accordingly:

$$MeOHcross_{over} = MeOH_{cir-in/out} - MeOH_{rxn} \tag{7}$$

In Eq. 7, $MeOH_{cir\text{-}in/out}$ is the difference in methanol volume at the inlet and outlet of the anode. From Eq. 7, equivalent current ($i_{pmtMeOH,}$ mA cm^{-2}) for methanol crossover from anode to cathode side was determined [53]. The aforesaid procedure was carried out under OCV condition, and corresponding methanol crossover rates were estimated. Based on the results of proton conductivity and methanol permeability, the electrochemical selectivity values for all the membranes were obtained using Eq. 8 as given below [53]:

$$\beta = \frac{\sigma}{\rho_{MeOH}} \tag{8}$$

In Eq. 8, ρ_{MeOH} is methanol permeability (cm^2 s^{-1}) and σ is proton conductivity (S cm^{-1}).

Membrane performance evaluation in DMFC

The aforesaid membranes' performance was evaluated in a DMFC by making membrane electrode assemblies (MEAs). In brief, 15 wt.% teflonized Toray-TGP-H-120 carbon paper of 0.37 mm in thickness was used as the backing layer. To prepare the gas diffusion layer (GDL), Vulcan XC-72R was suspended in cyclohexane and agitated in an ultrasonic water bath for 30 min. To this solution, 15 wt.% polytetrafluroethylene suspension in 2 ml

ammonia was added with continuous agitation to form slurry that was coated onto the backing layer uniformly until the required loading of 1.5 mg cm^{-2} carbon was obtained. GDL thus obtained was sintered in a muffle furnace at 350 °C for 30 min. For anode reaction layer, 60 wt.% Pt–Ru (1:1 atomic ratio) supported on Vulcan XC-72R carbon mixed with the binder and coated onto one of the GDL constituted the catalyst layer on the anode, while 40 wt.% Pt catalyst supported on Vulcan XC-72R carbon mixed with binder coated onto the other GDL constituted the catalyst layer on the cathode. The catalyst loading on both the anode and cathode was kept at 2 mg cm^{-2}. The active area for the DMFC was 4 cm^2. MEAs with Nafion-117, CS–PVA–SSA–Cs-stabilized SWA, and CS–PVA–GA-Cs-stabilized SWA membranes were prepared by sandwiching the aforesaid membranes between the two electrodes followed by hot pressing it at 130 °C for 3 min at a pressure of 60 kg cm^{-2}. MEAs were evaluated using a conventional fuel cell fixture with parallel serpentine flow field machined on graphite plates. The cells were tested at 70 °C with 2 M aqueous methanol under a flow rate of 2 ml min^{-1} at the anode side and oxygen at the cathode side under a flow rate of 300 ml min^{-1} at atmospheric pressure. Measurements of cell potential as a function of current density were conducted galvanostatically using a fuel cell test station (Model PEM-FCTS-158541) procured from Arbin Instruments (US).

Results and discussion

Additive stability for the membranes

From weight loss measurements presented in Fig. 1, it is clearly seen that the weight loss of SWA is more compared to the weight loss of Cs-stabilized SWA in the hybrid membrane with an error limit of 3%. Weight loss measurements quantified the efficacy of the modification technique in stabilizing the SWA within the polymer matrix. The weight loss of hybrid membrane with unmodified SWA is more in relation to the membrane with Cs-stabilized SWA, indicating greater stability of the latter with increased substitution of protons by Cs. More weight loss in case of hybrid membrane comprising unmodified SWA may be attributed to the leach out of SWA. Leaching of SWA was reduced due to the coulombic interaction between hydroxyl groups of membrane hybrid and caesium-stabilized SWA and also the formation of hydrogen bonds between blend and $[XM_{12}O_{40}]^{n-}$ anion of heteropoly acids, established through FT-IR, based on our earlier reported studies [21, 47, 48].

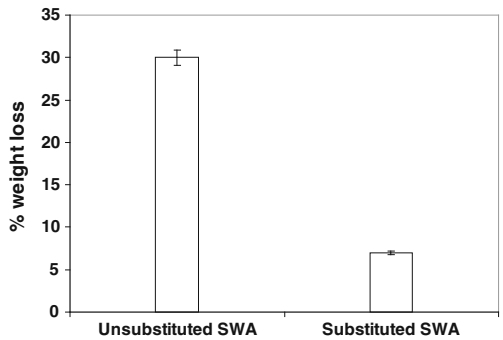

Fig. 1 Comparative weight loss between hybrid membranes containing unsubstituted and substituted SWA

Sorption for the membranes

Water sorption values for CS–PVA–SSA blend, CS–PVA–SSA–SWA hybrid membranes, CS–PVA–GA, and CS–PVA–GA–SWA hybrid membranes are presented in Fig. 2a, b, respectively. It is noteworthy that SSA-crosslinked membranes exhibited higher water uptake than GA-crosslinked

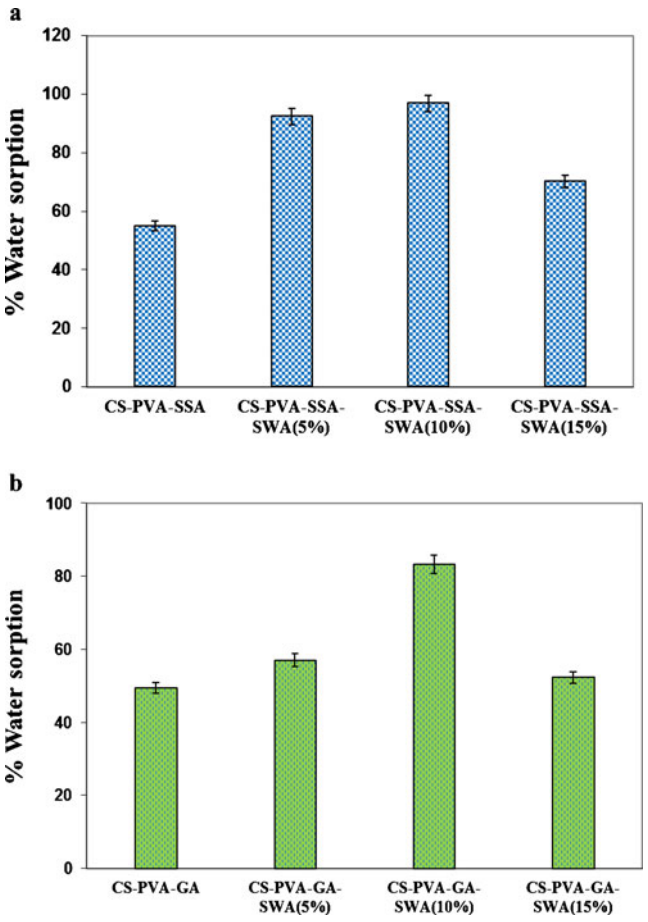

Fig. 2 **a** Percentage water sorption for CS–PVA–SSA blend and CS–PVA–SSA–SWA (5–15 wt.%) hybrid membranes. **b** Percentage water sorption for CS–PVA–GA blend and CS–PVA–GA–SWA (5–15 wt.%) hybrid membranes

membranes. This is due to the sulfonic acid groups of SSA that have enhanced the hydrophilicity in comparison to GA. The difference in water sorption between CS–PVA–SSA–SWA (5 wt.%) and CS–PVA–SSA–SWA (10 wt.%) is marginal, which could be due to the saturation reached in water sorption beyond 5 wt.% of SWA. The marginal difference in water sorption observed for CS–PVA–GA and CS–PVA–GA–SWA (5 wt.%) could be due to the initial resistance to water sorption by CS–PVA–GA compared to CS–PVA–GA–SWA because of the less hydrophilic nature of the former as evident from the difference in contact angle shown in Table 1. The decrease in water sorption observed in both hybrid membranes when 15 wt.% of SWA was incorporated in the membranes is due to the aggregation of particles and increased void defects as observed for most of polymer–inorganic composites studied in the literature [54, 55] and is evident from the surface and crosssectional SEM images shown in Fig. 4c, g, respectively.

It is noteworthy that, in both cases, when Cs-stabilized SWA is incorporated in the hybrid membrane, there is a dual hydrophilic interaction between SWA and a membrane hybrid, thereby increasing the degree of their swelling due to the distinct hydrated phase of SWA wherein the hydrated phases vary between 30 and 6 water molecules per SWA molecule due to the presence of Keggin cage [21, 24, 48, 49].

Proton conductivity for the membranes

The proton conductivities for all the aforesaid membranes increased with increase in temperature from 30 °C to100 °C as seen in Fig. 3a, b. It is noteworthy that the proton conductivity increases with increase in SWA content from 5 to 10 wt.% and decreases at 15 wt.% SWA. Higher content of SWA (>10 wt.%) in crosslinked CS–PVA blend disrupts the proton conduction path by blocking the voids of polymer matrix and decreases its proton conductivity as observed in the case of most of the inorganic fillers in the polymeric hybrid [49]. The observed ionic conductivity is also attributed to the water sorption data. The percentage water sorption of CS–PVA–SSA–SWA (10 wt.%) membrane is high. Generally, HPAs exhibit maximum proton conductivities at their maximum levels

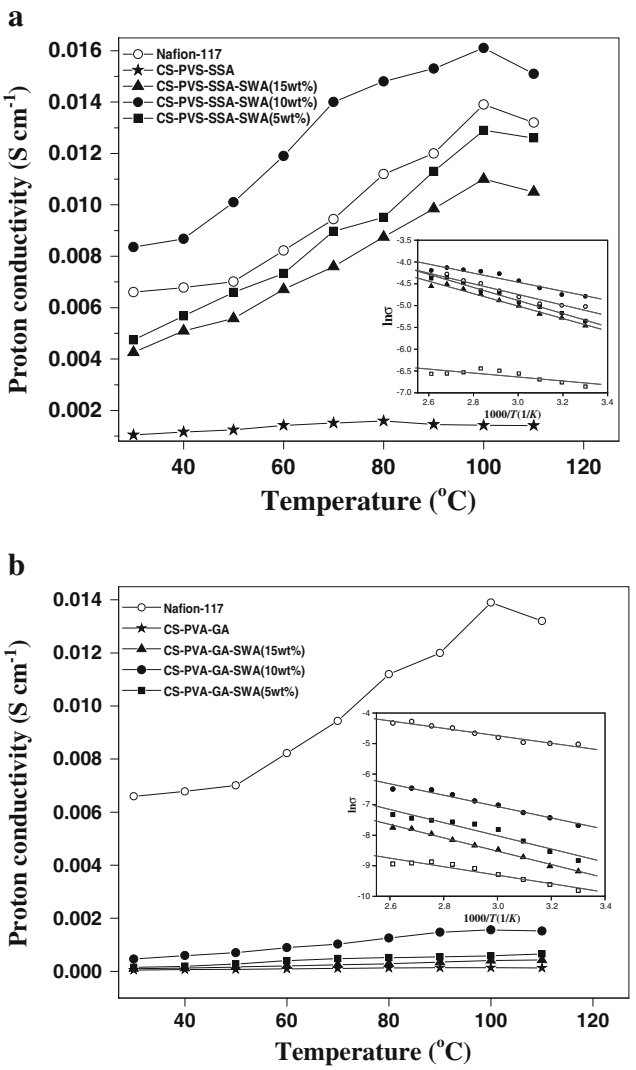

Fig. 3 **a** Proton conductivity vs. temperature and lnσ vs. 1,000/T plot of Nafion-117, CS–PVA–SSA blend, and CS–PVA–SSA–SWA (5–15 wt.%) hybrid membranes. **b** Proton conductivity vs. temperature and lnσ vs. 1,000/T plot of Nafion-117, CS–PVA–GA blend, and CS–PVA–GA–SWA (5–15 wt.%) hybrid membranes

Table 1 Properties of the membranes

Membrane type	Activation energy (kJ mol^{-1})	Tensile strength (MPa)	Percentage elongation (%)	Average contact angle (°)	Surface wetting energy (mN m^{-1})	Electrochemical selectivity, ×10^4 (S cm^{-3} s)	Area-specific resistance, R (Ω cm^2)
Nafion-117	7.46	18	32	76	17.47	1.51	0.62
CS–PVA–SSA	8.52	4	23.6	64	31.53	1.25	1.24
CS–PVA–SSA–SWA (10 wt.%)	4.58	9.6	17	49	46.95	2.69	0.16
CS–PVA–GA	17.05	4.5	24.8	68	26.98	0.94	1.55
CS–PVA–GA–SWA (10 wt.%)	9.06	8	11.8	57	39.30	1.38	0.88

of hydration due to their discrete ionic structures of fairly mobile basic structural units that exhibit extremely high proton mobilities [56, 57]. Effect of crosslinking can also be noticed through proton conductivity data. It can be clearly seen that SSA-crosslinked hybrid membranes show higher ionic conductivity than GA-crosslinked hybrid membranes due to the extra proton-conducting paths provided by the SSA. At room temperature, high water sorption helps protons to transport, suggesting involvement of intermolecular proton transfer during the mobility of protons, a process termed as structural diffusion (Grötthus mechanism). In all the hybrid membranes of CS–PVA–SWA, molecular diffusion (vehicular mechanism) dominates intermolecular proton transfer with increasing temperature [58, 59].

Inset to Fig. 3a, b shows the Arrhenius plots for the proton conductivity as a function of temperature for Nafion-117, CS–PVA–GA–SWA and CS–PVA–SSA–SWA hybrid membranes. It is noteworthy that activation energy is lower for CS–PVA–SWA hybrid than for Nafion-117 and crosslinked CS–PVA blend membranes as shown in Table 1, suggesting that lower energy is required for proton transport. All membranes exhibit Arrhenius-type temperature dependence and the energy required for proton transport is obtained from Eq. 9.

$$\sigma = \sigma_0 e^{-(E_a/RT)} \tag{9}$$

In Eq. 9, σ is the proton conductivity (S cm^{-1}), σ_0 is the pre-exponential factor, E_a is the activation energy in kJ mol^{-1}, R is the gas constant (8.314 $Jmol^{-1}$ K^{-1}), and T is the absolute temperature. The lower activation energy values observed for the hybrid membranes than the blend membranes suggests that the energy required to cross the barrier decreased, thereby allowing more of the protons to readily transport over the Eyring's energy barrier through the membrane as observed for similar hydrophilic membranes studied in the literature [60].

Mechanical properties of the membranes

The tensile strength values for Nafion-117, CS–PVA–GA, CS–PVA–SSA, CS–PVA–SSA–SWA, and CS–PVA–GA–SWA membranes in sorbed conditions are shown in Table 1. It is noteworthy that both tensile strength and percentage elongation are higher for Nafion-117 membrane because of its flexible chain mobility. However tensile strength and elongation are less for CS–PVA–GA and CS–PVA–SSA blend membranes because of the restriction in chain mobility. In contrast, for CS–PVA–GA–SWA and CS–PVA–SSA–SWA membranes, tensile strength has increased while percentage elongation decreased in comparison to blend membranes due to membrane rigidity by addition of SWA. SWA induces membrane rigidity, affecting its tensile strength and elongation at break [47, 61].

Scanning electron microscopy of the membranes

Figure 4a, c illustrates surface scanning electron micrographs for CS–PVA–SSA blend and CS–PVA–SSA–SWA hybrid membranes. CS–PVA–SSA–SWA hybrid membrane shows surface roughness due to the incorporation of SWA in the matrix in relation to the smooth morphology of crosslinked CS–PVA blend membrane. It can be seen from the crosssectional micrographs that voids of crosslinked CS–PVA matrix are filled by SWA and there is a molecular level distribution. Molecular level distribution is enhanced with increase in wt.% of SWA from 5 to 15 wt.% as seen in Fig. 4d–g. The morphology is in accordance with our earlier reports on similar kinds of blend membranes [62].

FT-IR analysis of the membranes

Figure 5 shows FTIR spectra for CS–PVA blend, GA crosslinked CS–PVA, and SSA crosslinked CS–PVA. The vibrational band observed between 2,820 and 3,000 cm^{-1} refers to the stretching of C–H from alkyl groups of PVA and the peak at 1,064 cm^{-1} is due to the stretching vibration in CS. Another broad band at 3,300–3,500 cm^{-1} is due to amine N–H symmetrical vibration or O–H stretching from the intermolecular and intramolecular hydrogen bonds of CS and PVA [63].

It is noteworthy that the band at 1,718 cm^{-1} corresponding to the C=O symmetric stretch of imide groups is due to crosslinking of CS–PVA with GA. CS–PVA blends have shown imine (−C=N–) band at 1,640 cm^{-1} and amine (N–H) band at 1,450 cm^{-1} after crosslinking with GA [63]. The CS–PVA–SSA blend membrane shows absorption band at 1,739 cm^{-1} characteristic of (C=O), and the band at 1,102 cm^{-1} is attributed to the stretch mode of C–O–C bond between alcohol groups of PVA and carboxyl groups of SSA. The absorption bands 1,161 and 1,021 cm^{-1} are attributed to $–SO_3$ group. This is in accordance with the bands observed for similar kinds of membranes studied earlier [64–66]. The stretching vibration of the CS–PVA blend also shifts to higher wavelength region after crosslinking with GA/SSA.

Thermal properties of the membranes

Three main degradation stages occur due to the processes of thermal dehydration, thermal degradation, and thermal decomposition of the polymeric membranes as shown in Fig. 6 [40, 46, 67, 68]. The first weight loss between 0 and 200 °C is due to the loss of absorbed water molecules from the CS–PVA–GA and CS–PVA–SSA matrix. The second weight loss between 200 and 450 °C is due to the thermal degradation of CS–PVA–GA and CS–PVA–SSA matrix. Decomposition of the main polymer chains and acetal

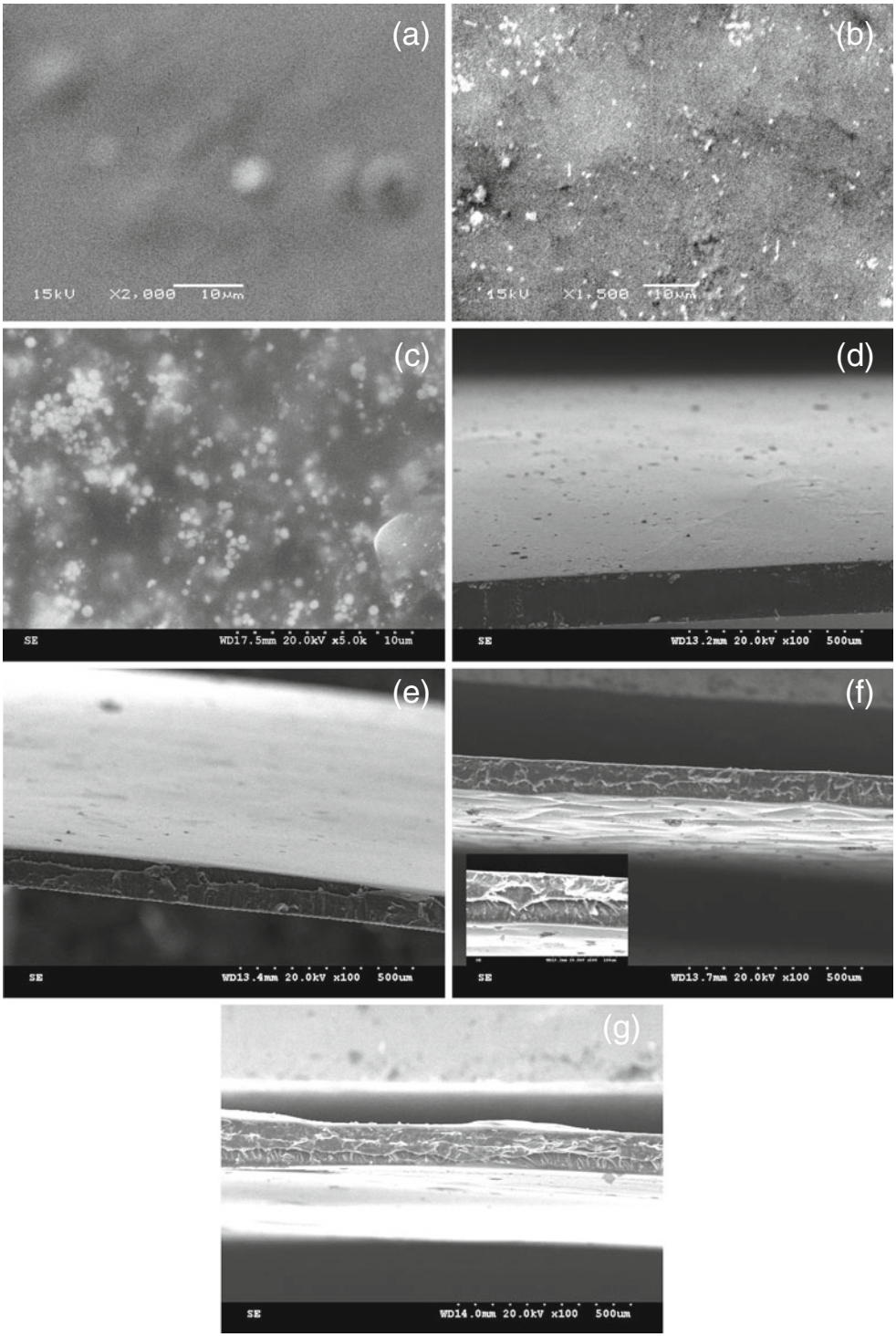

Fig. 4 Surface SEM micrographs for **a** CS–PVA–SSA blend, **b** CS–PVA–SSA–SWA (10 wt.%) and **c** CS–PVA–SSA–SWA (15 wt.%) and crosssectional SEM micrographs for **d** CS–PVA–SSA blend, **e** CS–PVA–SSA–SWA (5 wt.%), **f** CS–PVA–SSA–SWA (10 wt.%; *inset*, crosssection at higher magnification), and **g** CS–PVA–SSA–SWA (15 wt.%) hybrid membranes

linkage created during the crosslinking of GA in blend of CS–PVA–GA contributes to second weight loss, while in the case of CS–PVA–SSA membrane it is attributed to the loss of sulfonic acid due to the desulfonation of SSA and the resulting breakage of crosslinked bonds. The third weight loss observed between 450 and 800 °C is due to the decomposition of main chains of CS and PVA. However, in the case of CS–PVA–GA–SWA and CS–PVA–SSA–SWA hybrid, second weight loss may include the release of structural water from SWA and partial deprotonation, while third weight loss is for the decomposition of caesium salt of HPAs to metal oxides [69].

DTA for the membranes was performed in conjunction with TGA in the temperature range 0 to 400 °C to know the glass transition (T_g) and melting temperature (T_m) [68, 70] as shown in the inset of Fig. 6. The initial

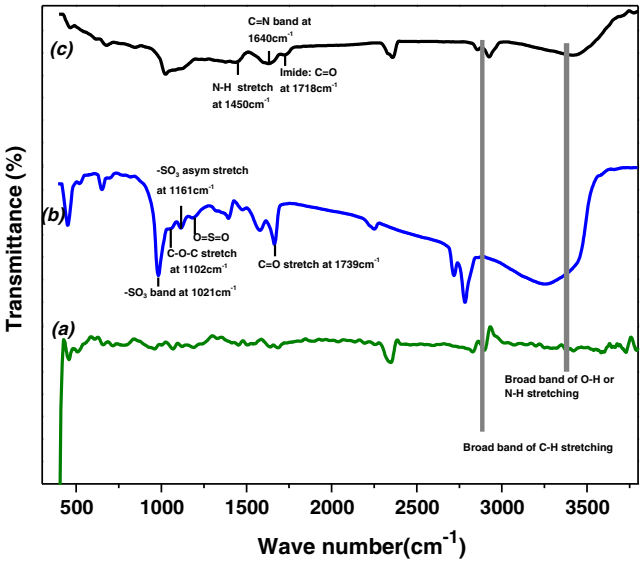

Fig. 5 FTIR plots for (*a*) CS–PVA, (*b*) CS–PVA–SSA, and (*c*) CS–PVA–GA blend membranes

(T_g) and final (T_m) endotherms of CS–PVA–SSA are 88 and 276 °C, while that for CS–PVA–GA blend membranes are 122 and 266 °C, respectively. The higher T_g observed for CS–PVA–GA indicates better thermal stability of this over CS–PVA–SSA.

Contact angle measurements for the membranes

Since liquid makes contact with the outermost molecular layer of a surface, contact angles are sensitive to chemical and physical changes that occur on the surface. It is also known that the surfaces of the multiphase polymer blends are heterogeneous and comprise different types of domains [71]. Table 1 shows the average contact angles and surface wetting energies for all the aforesaid membranes. The average contact angle decreases for the CS–PVA–SSA–SWA (10 wt.%) and CS–PVA–GA–SWA (10 wt.%) hybrid membranes than blend membranes, thereby increasing the surface wetting energy. This is due to the distinct hydrophilicity and hydrated phases of SWA [24]. In contrast, the contact angle for the CS–PVA–SSA and CS–PVA–GA blend is lower than that of Nafion-117 membrane because more hydrophilic chains are present in the blend. The hydrophilic interactions between CS and PVA affect the contact angle values varying as: Nafion-117>CS–PVA–GA>CS–PVA–SSA>CS–PVA–GA–SWA (10 wt.%)> CS–PVA–SSA–SWA (10 wt.%). The average contact angle for Nafion-117 is higher in comparison to all the membranes because of its hydrophobic fluorinated backbone that also decreases its surface wetting energy.

Methanol crossover and performance evaluation of membranes in DMFCs

The methanol crossover flux for Nafion-117, CS–PVA–GA, CS–PVA–SSA, CS–PVA–GA–SWA, and PVA-SSA-SWA hybrid membranes is presented in Fig. 7. The methanol crossover for the aforesaid membranes is measured under OCV condition at 70 °C. It is observed that the methanol crossover flux is lower for CS–PVA–GA–SWA (10 wt.%) and CS–PVA–SSA–SWA (10 wt.%) hybrid membranes in comparison to Nafion-117 and other membranes in the order: Nafion-117>CS–PVA–SSA>CS–PVA–GA>CS–PVA–SSA–SWA (10 wt.%)>CS–PVA–GA–SWA (10 wt.

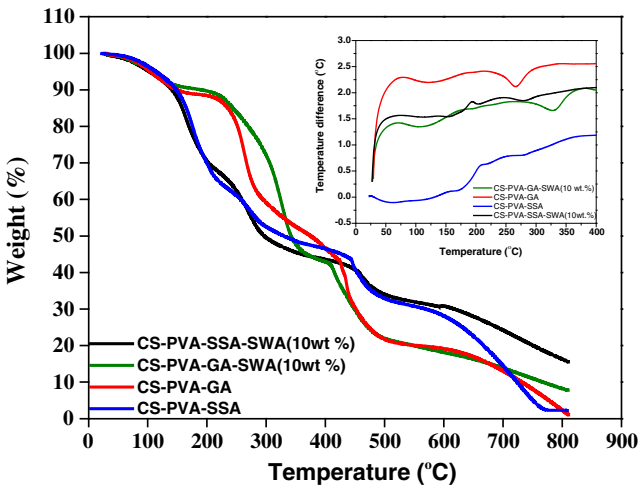

Fig. 6 TGA plots for CS–PVA–SSA blend, CS–PVA–SSA–SWA (10 wt.%), CS–PVA–GA, and CS–PVA–GA–SWA (10 wt.%) hybrid membranes. *Inset* represents DTA plots for CS–PVA–SSA and CS–PVA–GA blend membranes, and CS–PVA–SSA–SWA (10 wt.%) and CS–PVA–GA–SWA (10 wt.%) hybrid membranes

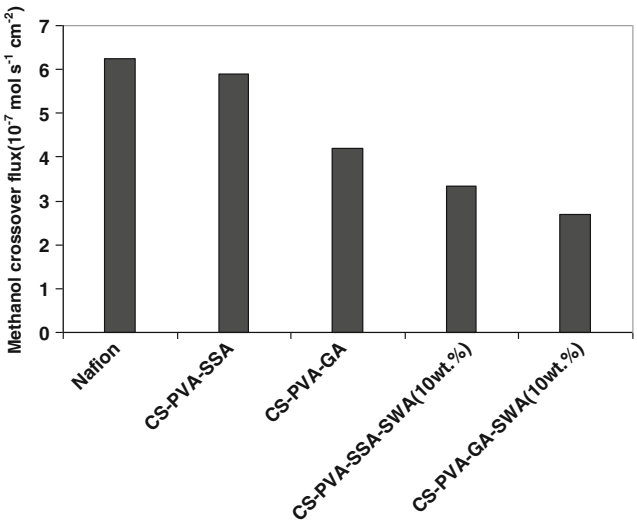

Fig. 7 Methanol crossover flux vs. current density plot of Nafion-117, CS–PVA–SSA, CS–PVA–GA blend, CS–PVA–SSA–SWA (10 wt.%), and CS–PVA–GA–SWA (10 wt.%) hybrid membranes under OCV conditions at 70 °C

%). This may be due to the formation of a dual-network structure between CS and PVA polymeric network, thereby restricting the larger methanol molecules to diffuse as shown in Scheme 1 (a and b). In the case of GA, crosslinking reaction takes place between –OH groups of the CS and PVA and –CHO groups of GA by forming the ether linkage, whereas in the case of SSA there is an introduction of negatively charged ion group in PVA by chemical modification through crosslinking with SSA. On the other hand, the amino groups of CS and sulfonate/carboxyl groups of SSA could provide coulombic interactions which result in electrostatic crosslinking of CS matrix. Such interactions are critical to achieve stable polyelectrolyte. SSA also acts as a donor of the hydrophilic $–SO_3H$ group through the polyelectrolyte [23, 33]. The methanol molecules may diffuse through the SO_3^- groups present in the CS–PVA backbone crosslinked by SSA which is associated with the hydrophilic nature of these polar sites. This can be controlled by incorporation of SWA to the dual network that is attributed to the columbic interaction between hydroxyl groups of crosslinked CS–PVA and stabilized SWA [72]. The hydrated phases of SWA restrict the methanol crossover from anode to cathode. It is noteworthy from Table 1 that the electrochemical selectivity for CS–PVA–SSA–SWA is the highest among all the membranes. The electrochemical selectivity of CS–PVA–GA blend membranes is lower compared to other membranes due to lower proton conductivity. However, methanol crossover for CS–PVA–SSA membranes is higher compared to that for CS–PVA–GA membranes, which in turn affects the balance between proton conductivity and methanol permeability. In contrast, the ratio is balanced for Nafion-117 and CS–PVA–SSA–SWA hybrid membranes. The larger molecular size and lesser polarity of the methanol molecule in relation to water also help in restricting methanol permeability through the hybrid membranes in DMFCs [40].

The cell polarization of MEAs fabricated with the aforesaid membranes is given in Fig. 8a, b respectively. Peak power densities of 156 mW cm^{-2} at a load current density of 400 mA cm^{-2} and 88 mW cm^{-2} at a load current density of 300 mA cm^{-2} were achieved for the MEAs

Scheme 1 **a** Dual network of CS–PVA–GA–SWA. **b** Dual network of CS–PVA–SSA–SWA

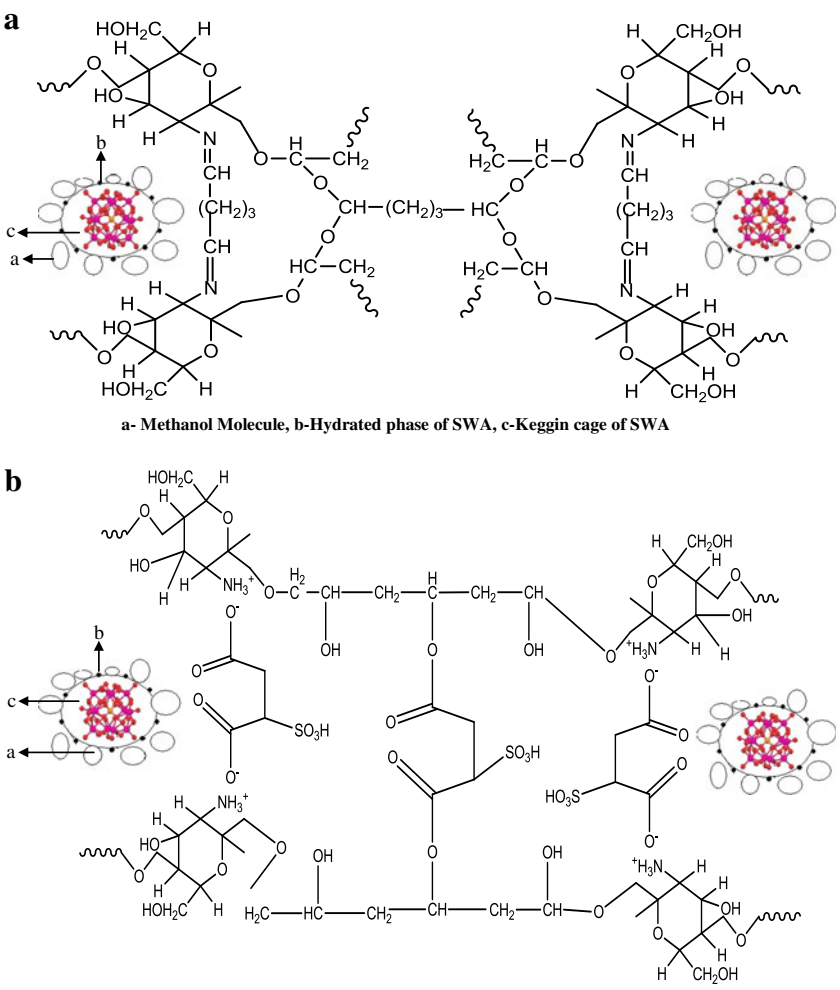

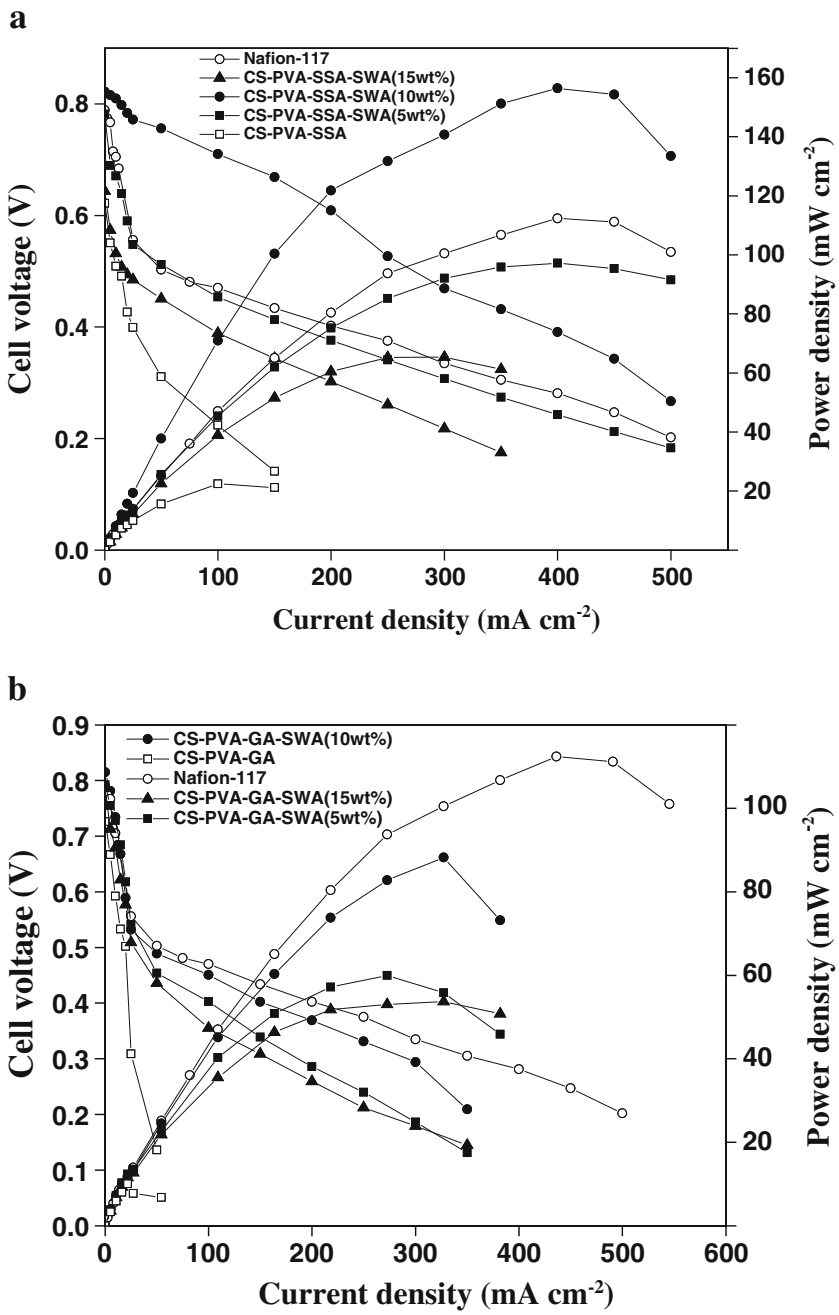

Fig. 8 **a** Voltage and power density vs. current density plot for Nafion-117, CS–PVA–SSA blend, and CS–PVA–SSA–SWA (5–15 wt.%) hybrid membranes. **b** Voltage and power density vs. current density plot for Nafion-117, CS–PVA–GA, and CS–PVA–GA–SWA (5–15 wt. %) hybrid membranes

comprising CS–PVA–SSA–SWA (10 wt.%) and CS–PVA–GA–SWA (10 wt.%) dual-network hybrid membranes as electrolytes, respectively. This is due to the higher proton conductivity of CS–PVA–SSA–SWA (10 wt.%) membrane. SWA has three protons available after the partial substitution of one H^+ ion with caesium in 1:0.5 molar ratio. By partially substituting one caesium ion and replacing one H^+ ion, the remaining three protons are left for proton conductivity. The higher DMFC performance observed for the hybrid membranes is due to the lower valence, electronegativity, and increased stability of Keggin type of anion in SWA structure that enhances its acid strength, thereby increasing proton conductivity [73].

It is noteworthy that area-specific resistance in the ohmic region of Fig. 8a, b and as seen in Table 1 is lower for CS–PVA–SSA–SWA (10 wt.%) membrane compared to Nafion-117. However, area-specific resistance is more for blend membranes than other membranes. This proves that ohmic loss is less for hybrid membranes in comparison to blend membranes. However, the durability of these membranes is a major challenge for its commercial viability. Studies to address these issues are under progress.

Conclusions

Hybrid dual-network membranes of natural and synthetic polymers with different compositions of SWA were fabricated and used for DMFC applications. The formation of a rigid dual network restricts methanol crossover and enhances the mechanical stability of the membrane. SSA-crosslinked membranes provide synergistic enhancement in proton conductivity and cell performance, whereas GA crosslinked membranes form a rigid structure that restricts methanol crossover.

Acknowledgements The authors thank CSIR, New Delhi, for providing financial support through DU-OLP-0058 EMPOWER Scheme and Supra-Institutional Project (SIP-18) under EFYP. We are grateful to Prof. A.K. Shukla for his constant guidance and advice in this work. We thank Tintula, Jalajakshi, and Arun for their valuable support. We also thank Mr. Ravishanker, CECRI-Karaikudi, for helping us in crosssectional SEM measurements.

References

1. Dillon R, Srinivasan S, Aricò AS, Antonucci V (2004) J Power Sources 127:112–126
2. Smitha B, Sridhar S, Khan AA (2005) J Membr Sci 259:10–26
3. Einsla Melinda L, Seung Kim Yu, Marilyn Hawley, Hae-Seung Lee, McGrath E, Baijun Liu James, Guiver Michael D, Pivovar Bryan S (2008) Chem Mater 20:5636–5642
4. Drioli E, Regina A, Casciola M, Oliveti A, Trotta F, Massari T (2004) J Membr Sci 228:139–148
5. Sinha PK, Mukherjee PP, Wang CY (2007) J Mater Chem 17:3089–3103
6. Shukla AK, Raman RK, Scott K (2005) Fuel cells 5:436–447
7. Scott K, Shukla AK (2007) Direct methanol fuel cells: fundamentals, problems and persepectives. In: White RE, Vayenas CG, Gamboa-Aldeco MA (eds) Modern aspects of electrochemistry. Springer, New York
8. Miyatake K, Tani H, Yamamoto K, Tsuchida K (1996) Macromolecules 29:6969–6971
9. Kundu PP, Sharma V, Yong GS (2007) Critical Rev Solid Stat Mater Sci 32:51–56
10. Nicholas WD, Yossef AE (2006) J Polym Sci Part B: Polym Phys 44:2201–2225
11. Ulbricht M (2006) Polymer 47:2217–2262
12. Joseph JG (2007) Polym Adv Technol 18:785–799
13. Rikukawa M, Sanui M (2000) Prog Polym Sci 25:1463–1502
14. Wu H, Zheng B, Zheng X, Wang J, Yuan W, Jiang Z (2007) J Power Sources 173:842–852
15. Yang CC, Lee YJ, Yang MJ (2009) J Power Sources 188:30–37
16. Mukoma P, Jooste BR, Vosloo HCM (2004) J Power Sources 136:16–24
17. Musale DA, Kumar A, Pleizier G (1999) J Membr Sci 154:163–173
18. Yang T, Zall RR (1984) J Food Sci 49:91–93
19. Anjali Devi D, Smitha B, Sridhar S, Aminabhavi TM (2005) J Membr Sci 262:91–99
20. Wang J, Zheng X, Wu H, Zheng B, Jiang Z, Hao X, Wang B (2008) J Power Sources 178:9–19
21. Zhiming C, Xing W, Liu C, Liao J, Zhang H (2009) J Power Sources 188:24–29
22. Smitha B, Sridhar S, Khan AA (2004) Macromolecules 37:2233–2239
23. Rhim JW, Park HB, Lee CS, Jun JH, Kim DS, Lee YM (2004) J Membr Sci 238:143–151
24. Kim DS, Park HB, Rhim JW, Lee YM (2004) J Membr Sci 240:37–48
25. Lin CW, Huang YF, Kannan AM (2007) J Power Sources 171:340–347
26. Ariyaskul AS, Huang RY, Douglas PL, Pal R, Feng X, Chen P, Liu L (2006) J Membr Sci 280:815–823
27. Zhou YS, Yang DZ, Chen XM, Xu Q, Nie Lu FM (2008) J Biomacromolecules 9:349–354
28. Yang JM, Su WY, Leu TL, Wang MC (2004) J Membr Sci 236:39–51
29. Wu LG, Zhu CL, Liu M (1994) J Membr Sci 90:199–205
30. Hennink WE, van Nostrum CF (2002) Advanced Drug Delivery Reviews 54:13–36
31. Manjanna KM, Pramod Kumar TM, Shivakumar B (2010) J Chem Tech Res 2:509–525
32. Gomez dAyala G, Malinconico M, Laurienzo P (2008) Molecules 13:2069–2106
33. Dashtimoghadam E, Sadrabadi MMH, Moaddel H (2010) Polym Adv Technol 21:726–734
34. Misono M (1987) Catal Rev Sci Eng 29:269–321
35. Kozhevnikov IV (1998) Chem Rev 98:171–198
36. Cui Z, Xing W, Liu C, Liao J, Zhang H (2009) J Power Sources 188:24–29
37. Lin CW, Thangamuthu R, Yang CJ (2005) J Membr Sci 253:23–31
38. Sauk J, Byun J, Kim H (2005) J Power Sources 143:136–141
39. Aparicio M, Mosa J, Etienne M, Durán A (2005) J Power Sources 145:231–236
40. Mohanapriya S, Bhat SD, Sahu AK, Pitchumani S, Sridhar P, Shukla AK (2009) Energy Environ Sci 2:1210–1216
41. Ukshe EA, Lenova LS, Korosteleva AI (1989) Solid State Ionics 36:219–223
42. Ramani V, Kunz HR, Fenton JM (2005) Electrochim Acta 50:1181–1187
43. Langpape M, Millet JMM, Ozkan US, Boudeulle M (1999) J Catal 181:80–90
44. Ramani V, Kunz HR, Fenton JM (2005) J Power Sources 152:182–188
45. Sahu AK, Selvarani G, Pitchumani S, Sridhar P, Shukla AK, Narayan N, Banarjee A, Chadrakumar N (2008) J Electrochem Soc 155:B686–B695
46. Bhat SD, Sahu AK, George C, Pitchumani S, Sridhar P, Chandrakumar N, Singh KK, Krishna N, Shukla AK (2009) J Membr Sci 340:73–83
47. Bhat SD, Sahu AK, Jalajakshi A, Pitchumani S, Sridhar P, George C, Banerjee A, Chandrakumar N, Shukla AK (2010) J Electrochem Soc 157:B1403–B1412
48. Mohanapriya S, Bhat SD, Sahu AK, Manokaran A, Vijayakumar R, Pitchumani S, Sridhar P, Shukla AK (2010) Energy Environ Sci 3:1746–1756
49. Mohanapriya S, Bhat SD, Sahu AK, Manokaran A, Pitchumani S, Sridhar P, Shukla AK (2009) J Bionanoscience 3:131–138
50. Soled S, Misceo G (1997) Mc Vicker WE, Gates A, Guiterrez, Paes J. Catal Today 36:441–450
51. Song KY, Lee HK, Kim HT (2007) Electrochim Acta 53:637–643
52. Perry RH, Green DW, Maloney JD (eds) (1997) Perry's chemical engineers handbook, 7th edn. McGraw-Hill, New York
53. Jiang R, Chu D (2004) J Electrochem Soc 151:A69–A76
54. Xu ZL, Yu LY, Han LF (2009) Front Chem Eng China 3:318–329
55. Guo R, Hu C, Pan F, Wu H, Jiang Z (2006) J Membr Sci 281:454–462

56. Horky A, Kherani NP, Xu G (2003) J Electrochem Soc 150: A1219–A1224
57. Ganapathy S, Fournier M, Paul JF, Delevoye L, Guelton M, Amoureux JP (2002) J Am Chem Soc 124:7821–7828
58. Kreuer KD (1996) Chem Mater 8:610–641
59. Kreuer KD (2001) J Membr Sci 18:29–39
60. Bhat SD, Aminabhavi TM (2007) J Membr Sci 306:173–185
61. Dai H, Guan R, Li C, Liu J (2007) Solid State Ionics 178:339–345
62. Meenakshi S, Bhat SD, Sahu AK, Sridhar P, Pitchumani S, Shukla AK (2011) J Appl Polym Sci. doi:10.1002/app.35522
63. Costa-Júnior ES, Barbosa-Stancioli EF, Mansur AAP, Vasconcelos WL, Mansur HS (2009) Carbohydr Polym 76:472–481
64. Lin CW, Huang YF, Kannan AM (2007) J Power Sources 164:449–456
65. Shao L, Lau CH, Chung TS (2009) Int J Hydrogen Energy 34:8716–8722
66. Shao L, Chung TS (2009) Int J Hydrogen Energy 34:6492–6504
67. Sahu AK, Selvarani G, Bhat SD, Pitchumani S, Sridhar P, Shukla AK, Narayan N, Banarjee A, Chadrakumar N (2008) J Membr Sci 319:298–305
68. Bhat SD, Manokaran A, Sahu AK, Pitchumani S, Sridhar P, Shukla AK (2009) J Appl Polym Sci 113:2605–2612
69. Kukino T, Kikuchi R, Takeguchi T, Matsui T, Eguchi K (2005) Solid State Ionics 176:1845–1848
70. Arvanitoyannis I, Kolokuris I, Nakayama A, Yamamoto N, Aiba S (1997) Carbohydrate Polym 34:9–19
71. Lin JC, Ouyang M, Fenton JM, Kunz HR, Koberstein JT, Cutlip MB (1998) J Appl Polym Sci 70:121–127
72. Okuhara T, Mizuno N, Misono M (1996) Advanced Synth Catal 41:113–122
73. Bardin BB, Bordawekar SV, Nerco M, Davis RJ (1998) J Phys Chem B 102:10817–10825